



**HAL**  
open science

## Thinned simulations of extremely energetic showers in dense media for radio applications

J. Alvarez-Muñiz, C.W. James, R.J. Protheroe, E. Zas

► **To cite this version:**

J. Alvarez-Muñiz, C.W. James, R.J. Protheroe, E. Zas. Thinned simulations of extremely energetic showers in dense media for radio applications. *Astroparticle Physics*, 2009, 32 (2), pp.100. 10.1016/j.astropartphys.2009.06.005 . hal-00598194

**HAL Id: hal-00598194**

**<https://hal.science/hal-00598194>**

Submitted on 5 Jun 2011

**HAL** is a multi-disciplinary open access archive for the deposit and dissemination of scientific research documents, whether they are published or not. The documents may come from teaching and research institutions in France or abroad, or from public or private research centers.

L'archive ouverte pluridisciplinaire **HAL**, est destinée au dépôt et à la diffusion de documents scientifiques de niveau recherche, publiés ou non, émanant des établissements d'enseignement et de recherche français ou étrangers, des laboratoires publics ou privés.

## Accepted Manuscript

Thinned simulations of extremely energetic showers in dense media for radio applications

J. Alvarez-Muñiz, C.W. James, R.J. Protheroe, E. Zas

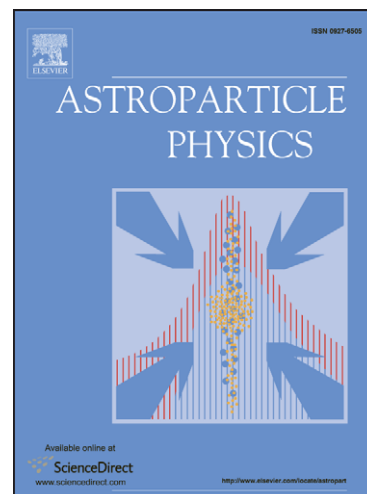
PII: S0927-6505(09)00102-9  
DOI: [10.1016/j.astropartphys.2009.06.005](https://doi.org/10.1016/j.astropartphys.2009.06.005)  
Reference: ASTPHY 1418

To appear in: *Astroparticle Physics*

Received Date: 27 February 2009  
Revised Date: 26 June 2009  
Accepted Date: 26 June 2009

Please cite this article as: J. Alvarez-Muñiz, C.W. James, R.J. Protheroe, E. Zas, Thinned simulations of extremely energetic showers in dense media for radio applications, *Astroparticle Physics* (2009), doi: [10.1016/j.astropartphys.2009.06.005](https://doi.org/10.1016/j.astropartphys.2009.06.005)

This is a PDF file of an unedited manuscript that has been accepted for publication. As a service to our customers we are providing this early version of the manuscript. The manuscript will undergo copyediting, typesetting, and review of the resulting proof before it is published in its final form. Please note that during the production process errors may be discovered which could affect the content, and all legal disclaimers that apply to the journal pertain.



# Thinned simulations of extremely energetic showers in dense media for radio applications

J. Alvarez-Muñiz,<sup>a</sup> C. W. James,<sup>b</sup> R. J. Protheroe,<sup>b</sup> E. Zas<sup>a</sup>

<sup>a</sup>*Depto. de Física de Partículas & Instituto Galego de Física de Altas Enerxías, Universidade de Santiago de Compostela, 15782 Santiago de Compostela, Spain*

<sup>b</sup>*Department of Physics, School of Chemistry & Physics, University of Adelaide, SA 5005, Australia*

---

## Abstract

This paper presents our results for full 3-D simulations of very-high to ultra-high energy electromagnetic cascades – and the associated coherent Cherenkov radiation – as might be produced by high-energy neutrino interactions in dense media. Using “thinning” techniques, we develop an algorithm based on the existing “ZHS” code, and demonstrate that the new “ZHS-thinned” code can produce fast and accurate results for showers up to  $10^{20}$  eV. Using ZHS-thinned, we develop new parameterisations for the radiation from showers in ice, salt, and the lunar regolith, with a separate treatment of the megaregolith (deep regolith). Our parameterisations include for the first time a method to simulate fluctuations in shower length induced by the LPM effect. Our results, which avoid the pit-falls of scaling simulations from lower energies, allow improved calculations of the detection probability for experiments searching for high-energy neutrinos using the radio technique.

*Key words:* high energy cosmic rays and neutrinos, high energy showers, Cherenkov radio emission

*PACS:* 95.85.Bh, 95.85.Ry, 29.40.-n,

---

## 1 Introduction

The search for neutrinos of EeV-scale energies is motivated by observations of the highest-energy cosmic rays, with the expectation that the detection of these neutrinos will help identify the sources of cosmic rays at these energies, as well as providing insight into the highest-energy astro- and particle-physics [1–3].

A very promising method to detect high-energy particle interactions in dense media was first proposed by G. A. Askaryan in the 1960’s [4]. By remotely

detecting the coherent Cherenkov (microwave-radio) radiation produced from the excess of electrons in the cascade of particles resulting from a high-energy particle interaction in a medium transparent to radio waves, the need to directly instrument large volumes to search for particles with extremely low fluxes and/or interaction cross-sections is obviated. As the energy in the radiation scales with the square of primary particle energy, this method naturally lends itself to detecting the highest energy neutrinos and cosmic rays. Starting from the first pioneering experiments using the radio technique (RICE [5] and Parkes [6]), the number and range of experiments has grown steadily, and now encompasses the Antarctic *in-situ* ice experiment RICE and balloon experiment ANITA [7], and projects observing the Moon with ground-based radio-telescopes such as GLUE [8], NuMoon [9] and LUNASKA [10].

In order to measure the properties of the primary particle, the observed spectrum of Cherenkov radiation must be related back to the properties of the induced cascade. This in turn requires a detailed knowledge of the magnitude, angular distribution and the frequency-dependence of the emitted Cherenkov radiation. Originally calculated using Monte Carlo techniques, the radiated spectrum from purely electromagnetic showers has been directly measured at particle accelerators. Coherent Cherenkov radiation produced by a beam of particles was first observed in tests performed at the Argonne Wakefield Accelerator [11]. The experimental confirmation of the Askaryan effect came later in a series of experiments at SLAC, first in silica sand [12,13] and then in rock salt [14] and ice [15], with results in good agreement with the theoretical calculations [16]. However, to achieve EeV-energy showers in a laboratory requires bunches of a large number of relatively low energy particles, and the resulting cascade of secondaries has neither the same spatial structure as a shower arising from a single ultra-high energy (UHE) particle nor the same expected spectrum and angular distribution of the emitted Cherenkov radiation. Additionally, a wide range of materials have been proposed as suitable dense media for the detection of the Askaryan effect, including ice, rock salt, and the various layers of the lunar regolith, and in some cases (notably the latter) direct measurement is not possible. This calls for accurate simulations of the spectrum of coherent Cherenkov radiation from EeV showers over a wide range of media.

Full calculations of coherent Cherenkov radiation from simulated electromagnetic cascades are very computationally intensive. Particles have to be tracked down to sub-MeV energies where the bulk of the radiation is known to be produced [17], so that even a 1 TeV shower comprises of the order of  $10^6$  particles (in total) to be tracked. Tracking all  $10^{12}$  particles expected in a single EeV shower is infeasible with current technology. A parameterisation of the emitted radiation in ice at EeV energies was performed in the past exploiting the analogy with diffraction by a single slit by Fourier-transforming an approximate longitudinal and lateral profile of the shower [18–20]. Results for other

media were obtained using simple scaling relationships, which at TeV energies and for the regolith differ by  $\sim 30\%$  from the results obtained in full Monte Carlo simulations [16].

There is a clear need to develop a fast code to fully simulate electromagnetic showers in 3-D at EeV energies and above in an arbitrary dense medium. Here, we investigate thinning techniques [21,22] as a method to reduce the computer time, and apply them to the ZHS code [17]. This is a well-known and well-tested code [23] originally developed for the simulation of electromagnetic showers in ice and the calculation of the associated Cherenkov emission at MHz-GHz frequencies. Thinning techniques involve following only a small, representative fraction of the particles in a shower, and assigning to each tracked particle a corresponding weight to compensate for the rejected particles. In the first section of this paper, we develop a thinning algorithm appropriate to the calculation of coherent Cherenkov radiation, and implement it in the ZHS electromagnetic code to produce the “ZHS-thinned” code. The behaviour of the new “ZHS-thinned” code is analysed using two independent techniques, and we test its ability to reproduce key quantities over a broad energy range such as excess tracklength, shower length along the shower axis, and width in the direction perpendicular to the shower axis, as well as the frequency spectrum and angular distribution of the coherent Cherenkov electric field.

In the second section, we use the ZHS-thinned code to develop new parameterisations of coherent Cherenkov radiation from electromagnetic showers at and above EeV energies for a wide range of media, which extends the work of [16] to energies above those at which the Landau-Pomeranchuk-Migdal (LPM [24]) effect becomes important. This includes a first parameterisation for the deep regolith (“megaregolith”) of the lunar highlands, which is relevant for lunar observations utilising low frequencies which could probe the sub-regolith layers (see Ref. [25] and references contained therein). The scaling relationships of the electric field with medium parameters obtained in previous works [16] are tested by comparison of our results in the lunar regolith and megaregolith, which have the same composition but different densities and refractive indices, both of which change smoothly with depth. This is also the case for Antarctic ice. In both of these media, where discrete parameterisations for fixed density or refractive index are inappropriate, our testing of the scaling relationships will be most relevant.

## 2 Thinning Electromagnetic Showers

Thinning methods have been applied successfully and extensively to high-energy air-shower simulations [21,22,26]. Due to the different physical pro-

cesses of interest in the radio-technique, we do not expect to be able to directly implement results on thinning from air-shower applications. For instance, thinning methods suitable for simulating air shower detection at ground level aim at reducing the number of tracked particles near the core — usually not observed in surface detectors — while maximising the tracking of particles that hit the ground far from the core. For radio applications Cherenkov radiation is produced by the charged particles at essentially all stages in the shower development, close and far from shower axis. Despite this fact many of the principles of thinning already developed for air shower physics are broadly applicable, and thus we develop our methodology in a similar manner.

### 2.1 The ZHS code

The ZHS code [17] generates electromagnetic showers from a  $e^\pm$  or  $\gamma$  primary particle, follows secondary particles of sufficient energy to produce Cherenkov radiation<sup>1</sup>, and passes the particle tracks generated to a routine to calculate the spectrum radiated. Initially developed to work in ice, showers — and associated Cherenkov electric fields — can be simulated in different media using the latest version of the code, simply by specifying the composition, density, and refractive index for radio frequencies of the medium in consideration. The necessary division of the (effectively continuous) particle paths into piecewise linear tracks can be performed in various ways, with shorter divisions allowing increasingly accurate parameterisations to higher frequencies at the expense of computer time [23]. For our purposes it suffices to choose tracks between significant discrete interactions, defined here as the bremsstrahlung emission of a  $E \gtrsim 100$  keV photon and pair production, Moeller, Bhabha and Compton scatterings. This method is accurate up to  $\sim 10$  GHz, above the frequency at which the coherent behaviour of the emitted signal is expected to break down in all of the media considered in this work [16]. Shorter tracks will lead to a significant increase in computing time but at no improvement in accuracy. Particles of energy below the Cherenkov threshold are discarded.

We adopt the same definition as in [17] of the Fourier transform of the electric field from the time domain to the frequency  $\nu = \omega/2\pi$  domain:

$$\vec{E}(\vec{x}, \nu) = 2 \int_{-\infty}^{\infty} dt e^{i2\pi\nu t} \vec{E}(\vec{x}, t) \quad (1)$$

<sup>1</sup> Down to the Cherenkov threshold kinetic energy  $E_{\text{thresh}}$  of a few tens of keV to 100 keV, depending on the medium and particle in question.

The inverse transformation is given by,

$$\vec{E}(\vec{x}, t) = \frac{1}{2} \int_{-\infty}^{\infty} d\nu e^{-i2\pi\nu t} \vec{E}(\vec{x}, \nu) \quad (2)$$

## 2.2 Thinning algorithms of electromagnetic showers for radio applications

In a purely electromagnetic code such as ZHS, every interaction can be characterised as  $A \rightarrow B + C$ , with energies  $E_A$ ,  $E_B$ , and  $E_C$ . At the heart of a thinning algorithm is a routine to choose which of the two secondary particles in an interaction to follow and which to discard, and what weights to assign to those followed. Our thinning algorithm is implemented whenever a significant interaction (as defined above) occurs, and in general will choose to follow particles  $B$  and/or  $C$  with probabilities  $p_B$  and  $p_C$ . If the parent particle  $A$  had weight  $W_A$ , the subsequent weight of  $B$  – and similarly for  $C$  – is  $W_B = W_A/p_B = w_B W_A$ , where we define  $w_B$  as the “weight increase”.

Coherent Cherenkov radiation results from an excess of electrons over positrons in the shower. This excess comes primarily from low-energy electrons knocked into the shower from the surrounding medium by shower photons, positrons and electrons, with a dearth of positrons due to annihilation (also at low energies) providing a secondary mechanism. The lateral spread of the shower is also governed chiefly by scattering of low-energy particles of tens of MeV. Conversely, the longitudinal profile is mainly determined by high energy interactions, and will exhibit elongation above the LPM energy of approximately 1 PeV, depending on the medium [27]. It is critical therefore that our thinning algorithm reproduces as accurately as possible both the high- and low-energy behaviour, since the lateral and longitudinal shower development determine the spectrum and angular distribution of the emitted radiation. Therefore, we follow the prescription of [22], and set both a maximum and minimum thinning threshold,  $E_{\max}$  and  $E_{\min}$ . This method also limits the weight on any individual particle, preventing undue variation; setting  $E_{\min} = 0$  replicates single-threshold thinning, while an unthinned shower also has  $E_{\max} = 0$ . We define the thinning level as  $f_L = E_{\max}/E_{\min}$ . We also define  $f_n = n_0/n$  as the ratio of the number of tracks explicitly accounted for in a fully simulated shower and in a thinned one. This is a platform-independent measure for the reduction in computing time  $t$ , since the most computationally-intensive routine is the Cherenkov radiation calculation, which is performed once for each particle track. Approximately  $f_n \simeq f_t = t_0/t$  where  $t_0$  and  $t$  are respectively the computing (CPU) time needed to simulate a full and a thinned shower. We also expect the computing-time reduction factor  $f_t \simeq f_n$  to be proportional to the thinning level  $f_L$ .

With these definitions and considerations, we can define the thinning algorithm:

- (1) If  $E_A$ ,  $E_B$  and  $E_C$  are all greater than  $E_{\max}$  or all lower than  $E_{\min}$ , then particles  $B$  and  $C$  are always tracked ( $p_B = p_C = 1$ ).
- (2) If  $E_A$ ,  $E_B$  and  $E_C \in (E_{\min}, E_{\max})$ , then either  $B$  or  $C$  (but never both of them) is accepted with probability  $p_B = E_B/E_A$  (and  $p_C = 1 - p_B$ ).
- (3) Finally, in any other case (those interactions where at least one of the thinning thresholds falls into the energy-range spanned by the interaction, i.e. any  $(E_{\min/\max}) \in (E_A, E_{B/C})$ ), an independent test is performed on each particle to determine which of the two are kept, so that in this case both, only one, or none of the two secondaries will be rejected. The probability  $p_p$  of retaining each particle with energy  $E_p$  is given by:

$$p_p = \begin{cases} 1 & \text{if } E_p > E_{\max}, \\ \frac{E_p}{E_{\max}} & \text{if } E_A > E_{\max} > E_p > E_{\min}, \\ \frac{E_{\min}}{E_A} & \text{if } E_{\max} > E_A > E_{\min} > E_p, \\ \frac{E_{\min}}{E_{\max}} & \text{if } E_A > E_{\max}, E_{\min} > E_p. \end{cases}$$

This thinning algorithm is essentially a logical extension to two thinning thresholds of the well-known Hillas thinning algorithm [21] which uses only one thinning threshold  $E_{\text{th}}$ . In fact by setting  $E_{\min} = 0$  and  $E_{\max} = E_{\text{th}}$  one recovers the original Hillas algorithm.

There are several advantages of this thinning algorithm that are worth commenting on. Firstly, the weights cannot exceed the thinning level  $f_L$ , and the number of low-energy particles is reduced also by a factor  $f_L$ . This ensures that no individual particle can have too great an influence over the shower parameters. Another advantage is that while secondary particles  $B$  and  $C$  are above  $E_{\max}$  or below  $E_{\min}$  no further thinning is performed, allowing a good description of the high- and low-energy particles which are relevant for shower development and charge excess generation respectively as discussed above. Finally, the time reduction should behave predictably, since the greatest number of particles in the shower are generated at low energies, and the most demanding routine in the ZHS code is the calculation of the Cherenkov radiation over a grid of frequencies and observation angles. Thinning over a factor of  $f_L$  in energy should reduce the number of particles with energies below  $E_{\min}$  by the same factor. Thus we expect that total time taken to be  $f_L$  times smaller than that of an unthinned shower.

Note that in case (2) – when  $E_A$ ,  $E_B$  and  $E_C \in (E_{\min}, E_{\max})$  – energy is conserved explicitly, and obviously in case (1) also. In case (3) however neither energy nor particle number will be conserved explicitly at each vertex, though they will still be conserved statistically after averaging over many interactions.

Quantity	$T$	$\langle r \rangle$	$M_r$	$\bar{z}$	$\langle z \rangle$	$M_z$
Def: $\sum_i$	$T_i$	$\frac{T_i}{T} \sqrt{x_i^2 + y_i^2}$	$\frac{T_i}{T} (x_i^2 + y_i^2)$	$\frac{T_i}{T} z_i$	$\frac{T_i}{T}  z_i - \bar{z} $	$\frac{T_i}{T} (z_i - \bar{z})^2$

Table 1

Definitions of variables used to assess the accuracy of our thinning routine. The sums in the formulas run over all particles in the shower.  $T_i$  is the tracklength of each particle (–ve for positrons, +ve for electrons, so the excess is a positive quantity) located at mean position  $(x_i, y_i, z_i)$ , where  $x = y = 0$  corresponds to a particle traveling along the shower axis.

We used this procedure, dubbed the “standard thinning algorithm” because of its well-defined thinning boundaries, as a standard yardstick. “Alternative thinning algorithms” involve forcibly conserving energy and particle number explicitly at every vertex. A possibility would be to thin when  $E_A$ ,  $E_B$  and  $E_C \in (E_{\min}, E_{\max})$  in the same way as in item (2) in the previous thinning algorithm, and not to thin in any other case. In this case for a given  $f_L$ , the fraction of particles explicitly tracked will be larger than in the standard thinning algorithm, since interactions spanning a thinning threshold will not be thinned.

We have implemented the standard thinning algorithm (energy not conserved explicitly) and the alternative thinning algorithm (energy forced to be conserved) into the ZHS code. A comparison between their performance is presented in the next section.

### 3 Testing Thinning Methods

Our goal with the introduction of thinning in the simulations of Cherenkov radio emission from high energy showers is to reproduce the spectrum and angular distribution of Cherenkov radiation predicted in full simulations as accurately as possible while at the same time minimising the computing time. Since the spectrum of Cherenkov radiation is approximately the Fourier transform of the distribution of excess negative charge [19,20], we assess the goodness of the thinning algorithms based on their ability to reproduce this distribution, reflected by the parameter set defined in Table 1. Of these, total excess tracklength  $T$  is the most useful, since it has very low intrinsic variability, and scales with the primary particle energy. Also defined is the shower “centre” at  $(\bar{x} = 0, \bar{y} = 0, \bar{z})$ , and the means (linearly-weighted variation) and “moments” (quadratically-weighted variation) of both shower length ( $\langle z \rangle$ ,  $M_z$ ) about the shower centre  $\bar{z}$ , and shower width ( $\langle r \rangle$ ,  $M_r$ ) about the shower axis ( $x = 0, y = 0$ ) in the direction perpendicular to the shower axis, all weighted by excess tracklength.

We measure the artificial variation in any given quantity introduced by the thinning algorithm using two methods. One is to generate a large number of thinned and unthinned showers, and compare the variation in (for example) excess tracklength  $T$  within the thinned showers to that of unthinned showers. Following [22], this allows the definition of the quality parameter  $Q_X$  for an arbitrary quantity  $X$  and a particular thinning level as  $Q_X \propto (t^{0.5} V_X)^{-1}$ , where  $t$  is the CPU time taken, and  $V_X$  is the relative variation (standard deviation) in the quantity  $X$ . Both  $t$ ,  $V_X$  and hence  $Q_X$  depend on the thinning level  $f_L$ . Here, we use the number of particle tracks  $n$  as proxy for CPU time, and normalise quality by that for an unthinned shower. Our definition then becomes:

$$Q_X = \frac{n_0^{0.5} V_X^0}{n^{0.5} V_X} \quad (3)$$

where  $V_X^0$  stands for the intrinsic variability of the quantity  $X$  in the set of unthinned showers. For a purely random quantity  $X$ ,  $Q_X = 1$ , since the variation  $V_X$  will go as  $n^{-0.5}$  and  $t$  goes as  $n$ . If the chosen thinning parameters are such that  $Q_X > 1$  then  $\bar{X}$  (the mean value of  $X$ ) is better estimated in a given time from the thinned showers, and on the contrary  $Q_X < 1$  means that the fully simulated showers give the best estimation. The selection process for a suitable thinning algorithm using this method involves choosing a set of thinning parameters (thinning level  $f_L$  and  $E_{\min}$ ) corresponding to computer-time constraints, and selecting those which give the highest quality parameter estimates for the set of relevant observables in Table 1.

The above method is relevant for estimating the mean properties of electromagnetic showers at a given energy. It cannot however determine the absolute accuracy in estimating a quantity  $X$  for an individual shower. To do this we have simultaneously run multiple copies of the same shower, each of them with different thinning parameters ( $f_L$ ,  $E_{\min}$ ) and/or algorithms. In this way we minimise the effect of the intrinsic shower fluctuations and we are confident that the differences in the values of the observables are solely due to the different thinning levels. For this purpose the ZHS code was modified to allow exactly the same shower tracks to be assigned different weights according to different thinning parameters and/or algorithms. Observables such as those in Table 1 estimated from the thinned showers can then be compared to their “true” (i.e. fully simulated) values. Optimal thinning parameters and/or algorithms can then be selected based on their attaining a desired level of accuracy and maximising time reduction. Here, we require a minimum level of accuracy of 10% between the thinned and the fully simulated showers, which is at the level of agreement between different cascade simulations below PeV energies [23].

### 3.1 Quality of Thinning

We have calculated the quality factor corresponding to different combinations of thinning parameters ( $f_L, E_{\min}$ ) and to the observables in Table 1 for primary shower energies of  $E_0 = 1$  TeV to  $E_0 = 10$  PeV, using one hundred showers for each energy and thinning parameter set.

The quality of length-related parameters  $Q_{\langle z \rangle}, Q_{M_z}$  was found to be the highest among the observables in Table 1 for all thinning parameters and algorithms, since length is determined by the high-energy component which remains unaffected by thinning. Conversely, the quality of total excess tracklength  $Q_T$ , and measures of width  $Q_{\langle r \rangle}$  and  $Q_{M_r}$ , were found to be the lowest, since these are governed by the low-energy (and thus most highly thinned) component on the shower. Excepting a very few cases, we found  $Q_T < \{Q_{\langle r \rangle}, Q_{M_r}\}$ , and therefore in this section we choose the worst possible case to select the optimal thinning parameters and use  $Q_T$  exclusively, keeping in mind that the quality factor of the other observables is almost always better.

In Fig. 1, we have plotted our results for  $Q_T$  against  $E_{\min}$  for 10 TeV and 1 PeV showers in ice. Two regimes for  $E_{\min}$  are clearly visible.  $Q_T$  decreases as  $E_{\min}^{-0.5}$  for  $E_{\min} \gtrsim 500$  MeV, and is stable with  $E_{\min}$  for  $E_{\min} \lesssim 500$  MeV. These two regimes are apparent in the whole energy range we have explored,  $1 \text{ TeV} < E_0 < 10 \text{ PeV}$ .

This behaviour arises because increasing  $E_{\min}$  reduces the thinning level – and hence the artificial variation due to thin sampling – proportionately, while the artificial variation associated with not enforcing energy conservation is essentially unaffected. Since increasing  $E_{\min}$  also proportionately increases the number of particles that are explicitly tracked (and hence the time taken),  $Q_T$  stays stable if the dominant component of artificial variation is due to thin sampling. However, for sufficiently large  $E_{\min}$ , variability due to not enforcing energy conservation will dominate<sup>2</sup>, so that  $Q_T$  will decrease as  $E_{\min}^{-0.5}$ . The turnover energy between  $E_{\min} = 500$  MeV and  $E_{\min} = 1$  GeV observed in Fig. 1 gives the point where the two components of artificial variation are equal. Altering either  $E_0$  or  $E_{\max}$  changes the contribution of both sources of variability equally, so the critical energy at which they equate is independent of both parameters.

Though we have a condition on  $E_{\min}$  so that the “standard thinning algorithm” produces maximum values of quality which are stable with  $E_{\min}$ , the question remains as to whether or not it is in fact a superior thinning algorithm. Since the “alternative thinning algorithm” forces conservation of energy by not thin-

<sup>2</sup> Energy is only conserved explicitly when  $E_A, E_B$  and  $E_C \in (E_{\min}, E_{\max})$

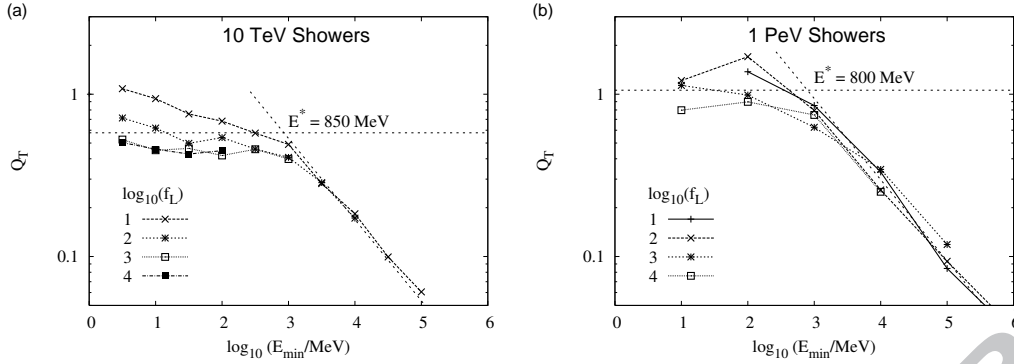


Fig. 1. Quality of total excess tracklength  $Q_T$  in (a) 10 TeV and (b) 1 PeV showers for various  $f_L$  as a function of  $E_{\min}$  using the standard algorithm. The (dotted) trend lines are found by fitting a constant  $k$  only to the range  $E_{\min} \leq 300$  MeV data for  $Q_T = k$  (horizontal dotted line), and  $E_{\min} \geq 3$  GeV for  $Q_T = k E_{\min}^{-0.5}$  (sloped line) — not all fitted points are shown for purposes of clarity. The  $Q_T = k E_{\min}^{-0.5}$  trend is clearly present for  $E_{\min} \gtrsim 1$  GeV.

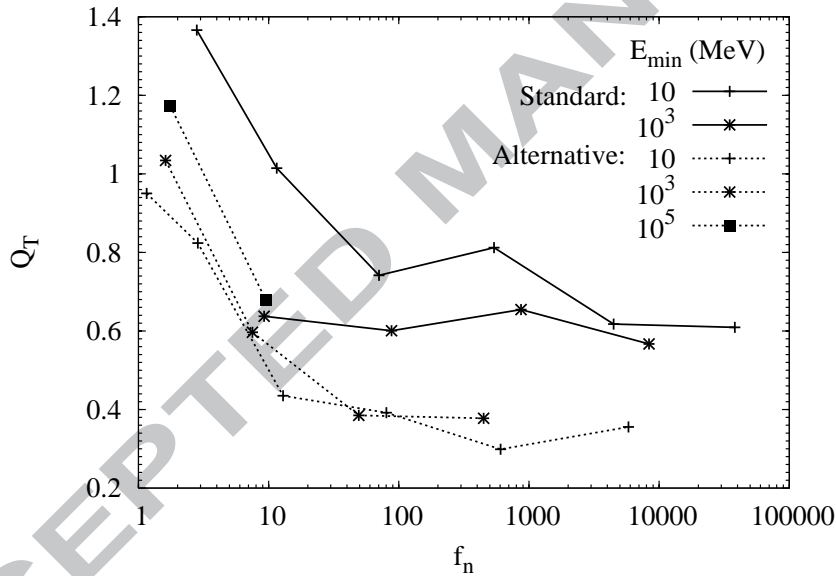


Fig. 2. Comparison of quality in total excess tracklength  $Q_T$  in 100 TeV showers between the two thinning algorithms, for the full range of thinning parameters ( $f_L, E_{\min}$ ), plotted as a function of  $f_n$  (see text). For each  $E_{\min}$ ,  $f_L$  is increasing to the right in factors of 10, beginning at  $f_L = 10$ .

ning over the thresholds, the time reduction will clearly be less than in the case of the standard thinning algorithm for a given set of thinning parameters. From our simulations we found that the alternative thinning routine forcing energy conservation explicitly takes between one and two orders of magnitude longer than the standard routine.

Given the difference between  $f_L$  and  $f_n$  (the actual reduction in computing time) for the two thinning algorithms, the quality  $Q_T$  of excess tracklength

must be compared in the context of  $f_n$ , since this is an actual measure of the time saved. We therefore plot  $Q_T$  against  $f_n$  in thinned 100 TeV showers using both algorithms, shown in Fig. 2. For the same reduction in computing time, the standard thinning algorithm provides a higher quality in  $T$  than the alternative algorithm, provided the condition  $E_{\min} \lesssim 500$  MeV is met, and even when  $E_{\min}$  is slightly greater, e.g. 1 GeV. These results held throughout the 1 TeV–10 PeV energy range studied. Therefore, we reject the alternative thinning algorithm, and proceed to analyse the standard thinning algorithm only for  $E_{\min} \lesssim 1$  GeV by simultaneously running the same shower with different thinning parameters.

At this stage we briefly summarize our findings:

- When  $E_{\min} < 1$  GeV, the quality factor  $Q_T \sim O(1)$  regardless of thinning level  $f_L$ .
- When  $E_{\min} > 1$  GeV for the standard algorithm, the quality factor  $Q_T < 1$  and declines rapidly with increasing  $E_{\min}$ .
- In the standard thinning algorithm (energy conserved statistically) the reduction in time is larger than in the alternative thinning algorithm (energy conserved explicitly at every vertex) for any given  $E_0, E_{\min}, f_L$ .
- For the same reduction in time, quality is better in the standard thinning routine (provided  $E_{\min} \leq 1$  GeV).
- The above conclusions hold for a wide energy range (1 TeV to 10 PeV) and different media, and the behaviour of the standard thinning routine is stable over this range.

### 3.2 Simultaneously running the same shower with different thinning parameters

We must now check to see that the structure of individual thinned showers is acceptably close to that of unthinned showers. Using thinning parameters  $E_{\min} < 1$  GeV and varying  $f_L$ , we compare the calculated values of  $T$ ,  $\langle r \rangle$ ,  $M_r$ ,  $\langle z \rangle$ , and  $M_z$  defined in Table 1, to those of *identical* fully simulated showers. For the combinations of  $(f_L, E_{\min})$  fulfilling the condition that all the above parameters differ from those obtained in identical fully-simulated showers by less than 10%, we choose those combinations producing the greatest reduction in CPU time. Defining  $f_0 = E_0/E_{\max}$  with  $E_0$  being the shower energy, we have found that optimal values correspond to  $f_0 \in (10^4, 10^5)$  with  $E_{\min} < 1$  GeV. These translate into optimal values of  $f_L$  depending on primary energy  $E_0$  given by:

$$f_L = f_0^{-1} \frac{E_0}{E_{\min}} \quad ; \quad E_{\min} < 1 \text{ GeV}. \quad (4)$$

$E_0$ [eV]	$f_L$	$E_{\min}$ [MeV]	$t$	$t_0/t$
$10^{14}$	1	0	2 hr 2.6 min	1.0
	10	10	43.7 min	2.8
	10	100	20.3 min	6.1
	100	10	10.7 min	11.5
	100	100	2.7 min	44.7
$10^{18}$	1	0	$\sim 2.33$ yr <sup>†</sup>	1.0
	$10^5$	10	4 h 33 min	$4.48 \cdot 10^3$
	$10^5$	100	41.8 min	$2.93 \cdot 10^4$
	$10^6$	10	31.9 min	$3.84 \cdot 10^4$
	$10^6$	100	4.7 min	$2.59 \cdot 10^5$

Table 2

CPU time gains through thinning, as a function of primary energy  $E_0$  and thinning parameters ( $f_L, E_{\min}$ ). The run-time  $t$  — given in years (yr), days (d), hours (hr) or minutes (min) — for both an unthinned ( $t = t_0, f_L = 1, E_{\min} = 0$ ) and for a thinned shower were calculated on a Intel Q6600 Quad processor 2.4 GHz, with Cherenkov radiation output on a moderately-sized grid of 15 angles by 30 frequencies. The time reduction factor is given by  $t_0/t$ . <sup>†</sup> For the  $E_0 = 1$  EeV shower the total time is estimated based on scaling CPU time linearly with primary energy  $E_0$ .

For instance, taking  $E_{\min} = 100$  MeV, and  $E_0 = 1$  EeV =  $10^{12}$  MeV, optimal values of  $f_L$  are in the range ( $10^5, 10^6$ ). Typical computational times for a range of showers using the optimal thinning parameters are shown in Table 2. Large reductions in time can be achieved, of the order of  $10^4 - 10^5$  at  $E_0 = 10^{18}$  eV. Characteristic accuracies of the parameters listed in Table 1 are given in Table 3. In the energy range below  $\sim 10$  PeV — in which full simulations are available — the accuracy of each parameter is computed by comparing thinned and full simulations of the same shower and averaging over many different showers. When full simulations are not feasible we check the stability of our results by comparing various optimally thinned simulations (with different thinning parameters) of the same shower between themselves.

In Fig. 3 we show the Cherenkov spectrum for 100 TeV showers simultaneously simulated both fully and with optimal thinning levels following Eq. (4). Above 1 PeV the calculation of the frequency spectrum for even a single unthinned shower is very time-consuming, so comparing thinned simulations to full ones is impractical. However, a useful check on thinning at energies above 1 PeV is to thin the same shower multiple times for different ( $E_{\min}, f_L$ ), and check for consistency and stability of the results when optimal thinning parameters given by Eq. (4) are applied. An example is shown in Fig. 4 in which the

$f_L$	$E_{\min}$	$\frac{\Delta T}{T}$ (%)	$\frac{\Delta r}{r}$ (%)	$\frac{\Delta M_r}{M_r}$ (%)	$\frac{\Delta z}{z}$ (%)	$\frac{\Delta M_z}{M_z}$ (%)
$E_0 = 10^{14}$ eV		$\bar{V}_X^0$ : intrinsic variation between fully simulated showers.				
1	0	0.21	0.19	0.44	4.1	7.8
$E_0 = 10^{14}$ eV		$\bar{V}_X$ : variation of thinned from fully simulated showers.				
10	10	0.19	0.7	1.5	0.15	0.3
10	100	0.5	1.0	3.4	0.25	0.5
100	10	0.7	2.2	7.8	0.5	0.95
100	100	1.9	3.3	10.5	0.9	1.7
$E_0 = 10^{18}$ eV		$\bar{V}'_X$ : variation between thinned showers only.				
$10^5$	10	0.23	0.65	2.4	0.16	0.3
$10^5$	100	0.55	0.95	3.3	0.28	0.55
$10^6$	10	0.65	2.2	7.5	0.5	0.9
$10^6$	100	1.55	2.9	9.5	0.65	1.4

Table 3

Variation in shower parameters (see Table 1) for sample optimal thinning parameters.  $\bar{V}_X^0$  is the variation in parameters *between* unthinned showers (the ‘intrinsic variation’);  $\bar{V}_X$  the variation of the parameters from simultaneous thinnings of the *same* shower about the unthinned (fully simulated) values (‘artificial variation’);  $\bar{V}'_X$  – used only at energies where full simulations become impossible – is the variation *between* simultaneous thinnings of the *same* shower (i.e. it estimates the artificial variation).

frequency spectrum at the Cherenkov angle for a 1 EeV shower was simulated using different combinations of  $E_{\min}$  and  $f_L$ .

Figs. 3 and 4 provide a more detailed check of the validity of the optimal thinning levels than the comparisons of the parameters listed in Table 1. Provided optimal combinations of  $E_{\min}$  and  $f_L$  (as given above) are used, the frequency spectra generated agree with that from fully simulated showers (Fig. 3) and other optimally-thinned simulations (Fig. 4) to within  $\sim 1\%$  below the roll-off in the frequency spectrum. At sufficiently high frequencies an accurate description of the electric field requires knowing the fine structure of the shower (even at the individual particle level), and clearly the thinning algorithms explored in this work are unable to account for it.

That our thinning algorithm behaves similarly over the energy range below 1 PeV in which full simulations are feasible, indicates that in fact Eq. (4) obtained for energies below 1 PeV can be extrapolated up into the EeV energy range. To further check this, we have also performed a hybrid simulation of

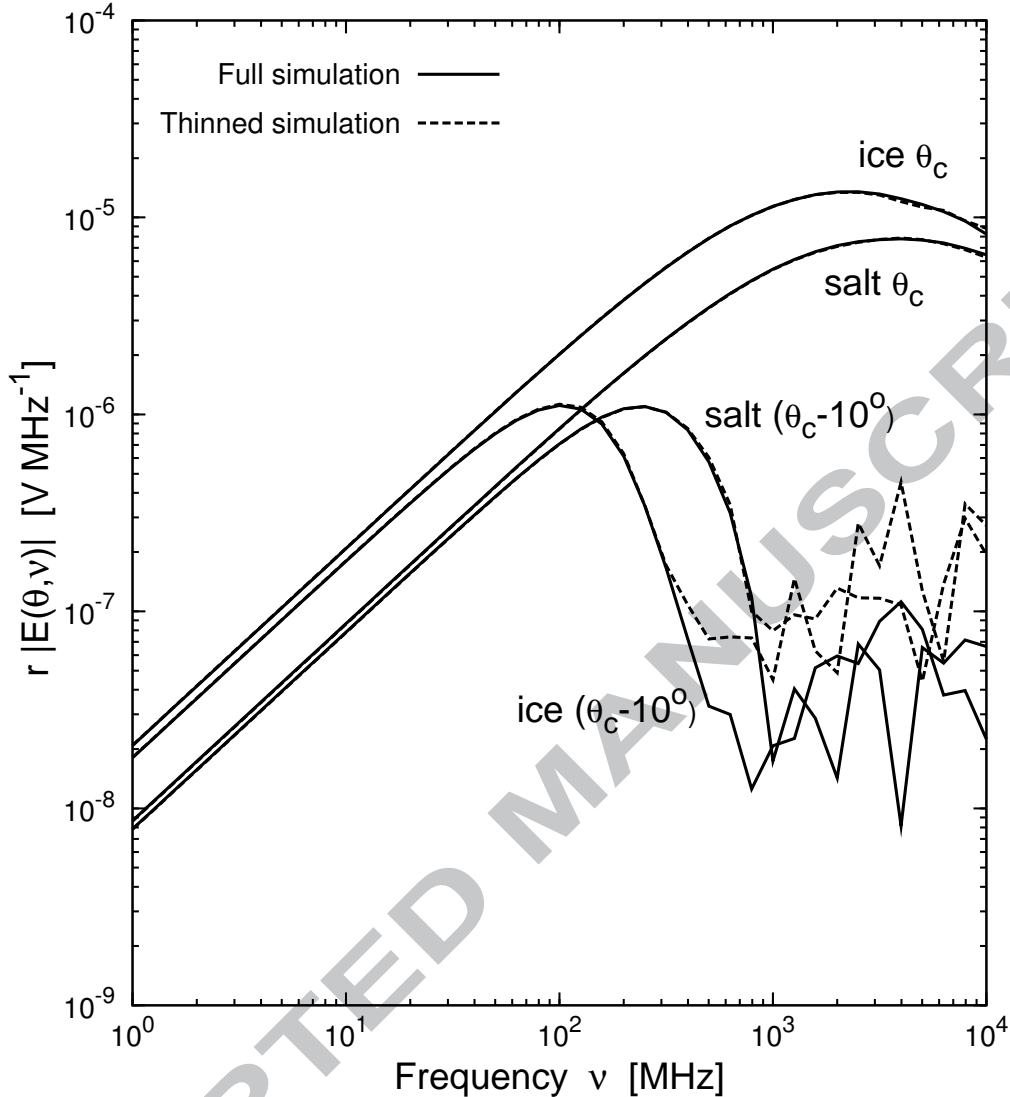


Fig. 3. Frequency distributions of coherent Cherenkov radiation calculated for electron-induced showers in ice and salt at 100 TeV primary energy at the Cherenkov angle ( $\theta_c$ ) and at  $10^\circ$  away from the Cherenkov angle. Solid line: full simulations; dashed line: thinned simulation with optimal parameters  $f_L = 10$  and  $E_{\min} = 100$  MeV as given by Eq. (4).

the longitudinal profile of the number of electrons and positrons in the shower, performed simultaneously with the thinned simulations in order to minimise the effect of the intrinsic shower fluctuations. The hybrid simulation tracks particles explicitly only if their energy is above an energy threshold, typically below the  $E_{\text{LPM}}$  scale of the medium. The longitudinal development of the secondary showers induced by particles below  $E_{\text{LPM}}$  is approximated using a Greisen parameterisation [28]. In this way the number of particles at each depth was calculated. In Fig. 5 we show the longitudinal development of a  $E_0 = 100$  EeV shower simulated with an optimal combination of thinning

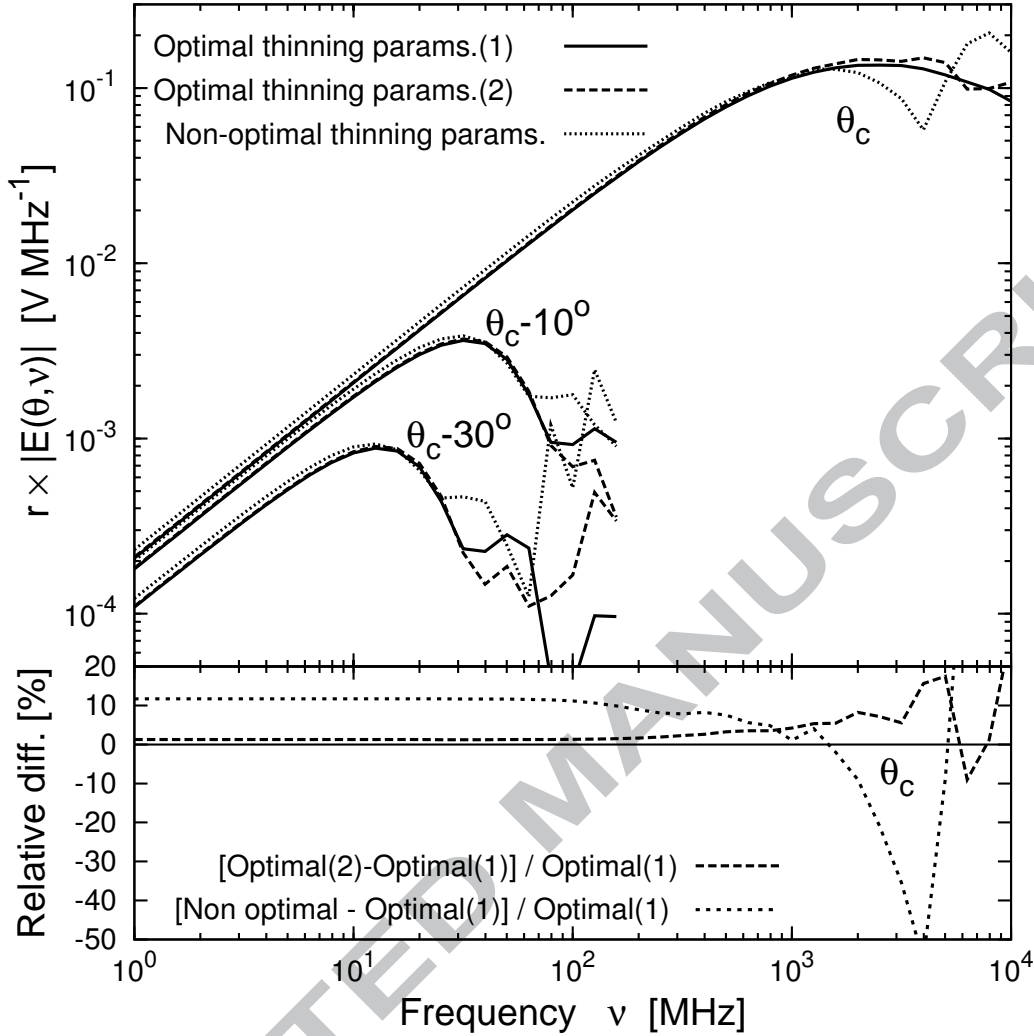


Fig. 4. Top panel: Frequency distributions of coherent Cherenkov radiation calculated for electron-induced showers in ice at 1 EeV primary energy for observation at the Cherenkov angle ( $\theta_c$ ), and  $10^\circ$  and  $30^\circ$  away from the Cherenkov angle for optimal and non-optimal thinned levels according to Eq. (4). Solid line: optimal thinning parameters (1)  $f_L = 10^5$  and  $E_{\min} = 100$  MeV; dashed line: optimal thinning parameters (2)  $f_L = 10^6$  and  $E_{\min} = 10$  MeV; dotted line: non-optimal thinning parameters  $f_L = 10^8$  and  $E_{\min} = 10$  MeV. Bottom panel: Relative difference in % between the electric field spectrum as obtained with the non-optimal (dotted line) and the set (2) of optimal parameters (dashed line) with respect to the electric field obtained with the set (1) of optimal parameters. For clarity only the relative differences for observation at the Cherenkov angle are shown.

parameters along with the result of the hybrid simulation. The agreement between both simulations of the development is remarkable and in particular the multi-peaked structure characteristic of showers in dense media with energies well above the LPM scale [29] is extremely well reproduced. This gives us confidence in the reliability of our thinned simulations.

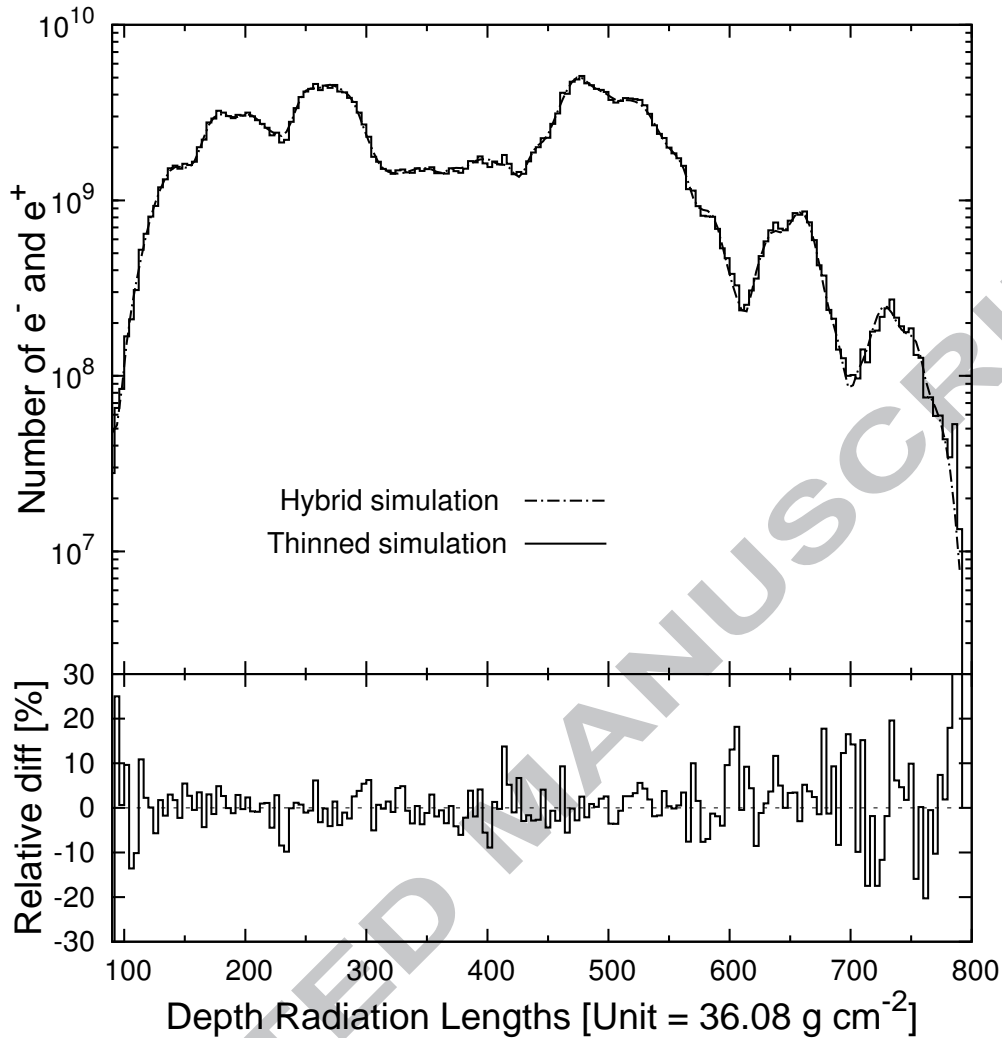


Fig. 5. Top panel: Distribution of the number of electrons and positrons along the shower axis for an electron-induced shower in ice with energy 100 EeV, calculated with a hybrid simulation (dashed line) and with a thinned simulation with optimal parameters  $f_L = 10^7$  and  $E_{\min} = 100$  MeV. Bottom panel: Relative difference in % between the hybrid and the thinned simulation as a function of depth calculated as thinned minus hybrid and normalized to the hybrid result.

So far, we have analysed results for ice only. This was done because ice was the first and historically the sole medium of experimental interest for radio-detection experiments. To check that our results are applicable to other media, we repeated the analysis above for salt (an example is shown in Fig. 3) and the lunar regolith and megaregolith. In all cases our conclusions (see below) were born out.

Summarising, we have found that the thinned showers generated by our thinning algorithm with optimal combinations of parameters reproduce the Cherenkov radiation spectrum from full simulations with an excellent degree of accuracy

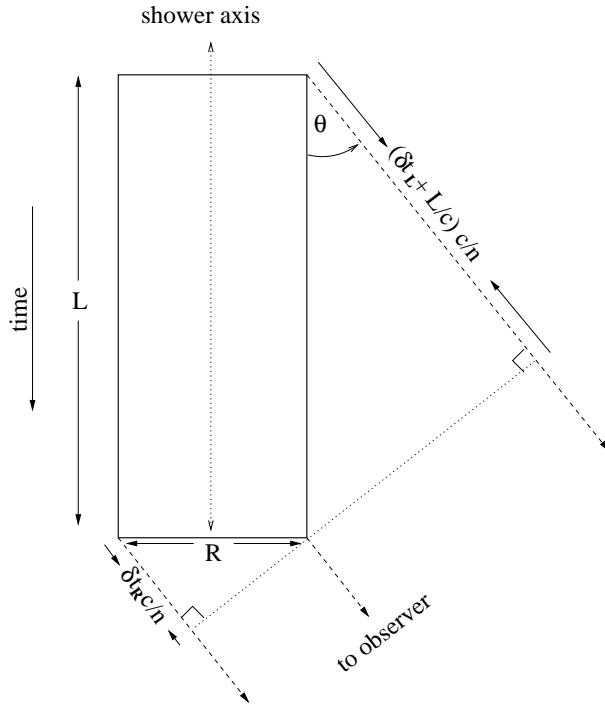


Fig. 6. The “box model” of shower development over the lifetime of the shower. A shower has an effective length  $L$  and width  $R$ , giving characteristic time delays of  $\delta t_L$  and  $\delta t_R$ . For  $\delta t_L = 0$ , we obtain the condition  $L \cos \theta = L/n$  for the Cherenkov angle  $\theta = \theta_C$ .

up to energies of  $\sim 1$  PeV. Above this energy full simulations become infeasible, but we have shown that the frequency spectra are internally consistent to within a few percent for individual showers. Moreover, a totally independent hybrid simulation gives results for the longitudinal development in very good agreement with the optimally thinned simulations. The time-reduction thinning allows at the highest energies is huge: whereas the radiated spectrum from a 100 EeV shower would have taken a few years to calculate with the standard ZHS routine, using our ZHS-thinned code we can now achieve acceptable accuracy in less than an hour. This enables us to run numerous showers of energies above 1 EeV, and we therefore develop parameterisations for the Cherenkov radiation produced based on these thinned showers for practical applications. This is the subject of the next section.

#### 4 Model and Parameterisation for Coherent Cherenkov Radiation from Electromagnetic Showers

The physical basis for our parameterisation of the radiated spectrum is the “box model” of shower development (Fig. 6), which has been used to explain the radiated spectrum from fully simulated showers at sub-LPM energies in a

variety of media [16,17,20]. In this model, the distribution of particle tracks making up the shower over its lifetime has a characteristic length  $L$  and width  $R$ , from which the resultant time delays  $\delta t_L$  and  $\delta t_R$  from radiation emitted over the length and breadth of the shower – with respect to a particle traveling along the shower axis at the speed of light – can be calculated with simple geometry (see Fig. 6) for any viewing angle. The condition  $\delta t_L = 0$  (no delays associated with the longitudinal spread of the shower) defines the Cherenkov angle  $\theta_C$ , so that interference over the width of the shower only (lateral decoherence) determines the spectral shape when the shower is viewed near  $\theta_C$ , while far from  $\theta_C$ , interference over the shower length (longitudinal decoherence) dominates [16]. The radiated spectrum  $\vec{E}(\nu)$  can then be described as a fully coherent amplitude  $A$  — increasing linearly with frequency — multiplied by lateral and longitudinal decoherence factors  $d_R$  and  $d_L$ , defined such that  $d_{R,L} \leq 1$  with  $d_{R,L} \rightarrow 1$  as  $\nu \rightarrow 0$ . Also,  $d_L \equiv 1$  at the Cherenkov angle  $\theta = \theta_C$ . In general,  $A$ ,  $d_L$  and  $d_R$  will be dependent upon the shower energy  $E_0$ , frequency  $\nu$ , and viewing angle  $\theta$  with respect to the shower axis, leading us to the following functional form:

$$r|\vec{E}(E_0, \theta, \nu)| = A(E_0, \theta, \nu) \times d_L(E_0, \theta, \nu) \times d_R(E_0, \theta, \nu) \quad (5)$$

where  $r$  is the (far-field) observation distance. In this paper, we always include both decoherence terms, although only for a small range of angles will both be relevant at the same time. We use the forms of Alvarez-Muñiz et al.[16] — given in Eq. (6) — for the decoherence factors, which have been shown to provide a good fit to the spectrum for showers with primary energies below  $E_{\text{LPM}}$ :

$$d_{R[L]} = \frac{1}{1 + (\nu/\nu_{R[L]})^{\bar{\alpha}[\bar{\beta}]}}. \quad (6)$$

Here,  $\nu_R$  and  $\nu_L$  are characteristic frequencies at which lateral and longitudinal decoherence become important, while  $\bar{\alpha}$  and  $\bar{\beta}$  give the strength of the decoherence. The frequencies  $\nu_L$  and  $\nu_R$  will be inversely proportional to the time delays  $\delta t_L$  and  $\delta t_R$ , which are in turn functions of  $L$  and  $R$ . The amplitude  $A$  of the fully coherent (low-frequency) component will be proportional to the total excess tracklength  $T$ . The proportionalities of  $L$ ,  $R$ , and  $T$  with properties of the interaction medium are well-established theoretical results [17,20,29,30]. We use the formalism of Alvarez-Muñiz et al. [16]:

$$\nu_L(\theta) \approx \frac{c}{L|1 - n \cos \theta|} = \frac{\rho}{k_L X_0 |1 - n \cos \theta|} \quad (7)$$

$$\nu_R(\theta = \theta_C) \approx \frac{c/n}{R} = \frac{\rho}{k_R R_M \sqrt{n^2 - 1}} \quad (8)$$

$$A(E_0, \theta, \nu) = \bar{k}_E \nu T \sin \theta \approx \bar{k}_E \frac{E_0}{E_C} \frac{X_0}{\rho} \nu \sin \theta \quad (9)$$

where the medium properties  $X_0$ ,  $n$ ,  $\rho$ ,  $R_M$  and  $E_C$  are respectively the radiation length ( $\text{g cm}^{-2}$ ), refractive index, density ( $\text{g cm}^{-3}$ ), Moliere radius ( $\text{g cm}^{-2}$ ), and critical energy (MeV).  $\bar{k}_L$ ,  $\bar{k}_R$ , and  $\bar{k}_E$  are proportionality constants. Throughout, we use the approximation  $\nu_R(\theta) = \nu_R(\theta_C)$ , since lateral decoherence is only important near the Cherenkov angle. Simulations by Alvarez-Muñiz et al. [16] in ice, salt, and the regolith have shown that variation in  $\bar{k}_L$  and  $\bar{k}_R$  between these media for showers at sub-LPM energies is of the order of 10%, while for  $\bar{k}_E$  it is of order 30%. Also, and as we have previously mentioned,  $L$  is dependent upon the shower energy  $E_0$ , so that the “constant”  $\bar{k}_L$  is in fact energy-dependent. For sufficiently low-energy showers, the dependence of  $L$  on  $E_0$  is small, while at energies where LPM-elongation is significant (typically for  $E_0 \gtrsim E_{\text{LPM}}$ ),  $L$  increases rapidly with  $E_0$  [27,29,31,32]. Thus we expect  $\bar{k}_L$  to be fit well by the following relation:

$$\bar{k}_L = \begin{cases} k_0 (E/E_{\text{LPM}}^*)^{\gamma_0} & E < E_{\text{LPM}}^* \\ k_0 (E/E_{\text{LPM}}^*)^{\gamma_1} & E > E_{\text{LPM}}^* \end{cases} \quad (10)$$

where  $k_0$ ,  $\gamma_0$  and  $\gamma_1$  are constants, and  $E_{\text{LPM}}^*$  is an effective energy – typically larger than  $E_{\text{LPM}}$  itself – at which LPM-elongation of the shower longitudinal profile begins to affect the emitted electric field. The quantities  $\bar{k}_E$  and  $\bar{k}_R$  are energy-independent however, since both excess tracklength and shower width are determined by low-energy interactions. Likewise, we expect  $\bar{\alpha}$  to be constant, while in general  $\bar{\beta}$  may vary at high energies as the shape of the shower changes. Note that while our toy model of shower development describes the shower as a box, our parameterisation Eqs. (5), (6) do *not* assume this shape, with the parameters  $\bar{\alpha}$  and  $\bar{\beta}$  related to the precise distribution of tracklength within the box.

Our fitting procedure is thus as follows. For each shower, we fit Eqs. (5) and (6) to the simulated spectrum at the Cherenkov angle for the parameters  $\bar{k}_E$ ,  $\nu_R$ , and  $\bar{\alpha}$  by setting  $d_L = 1$  ( $\nu_L \rightarrow \infty$ ), and we then relate  $\nu_R$  to  $\bar{k}_R$  via Eq. (8). Given these constraints, we allow  $\nu_L$  to vary, and then fit for  $\nu_L$  and  $\bar{\beta}$  at various angles away from the Cherenkov angle. Plotting the fitted  $\nu_L$  against  $\theta$  gives  $\bar{k}_L$  according to Eq. (7). We repeat this many times at each energy, and vary the energy in multiples of  $\sqrt{10}$  over the energy range 1 TeV to 100 EeV. Above this energy, the cross-section for photo-nuclear interactions becomes comparable to the pair-production and bremsstrahlung cross-sections [33], which is not included in the (purely electromagnetic) ZHS code. However, the energy range applicable to our calculations includes the full range of predictions for a GZK-flux of UHE neutrinos [35], while the relevance of UHE neutrino interactions above  $\sim 100$  EeV reduces as limits on models

predicting a flux of UHE  $\nu$  at energies above that from GZK interactions become stronger [7,8].

We repeat the above procedure in ice, salt, and the lunar regolith and megaregolith. The parameters for the first three are those of [16], while the megaregolith is treated as per Ref. [25] as regolith with refractive index 2.68 and density 3.0 g/cm<sup>3</sup>.

#### 4.1 Results for different media

The fitted parameters  $\bar{k}_E$ ,  $\bar{k}_R$ ,  $\bar{\alpha}$ ,  $\bar{\beta}$  for each medium are given in Table 4. For  $\bar{k}_L$ , we find the form given in Eq. (10) to be suitable, and the parameters defined therein are summarised in Table 5. We also find an upward trend in  $\bar{\beta}$  with energy for all media, consistent with the shower becoming more elongated and less singly-peaked. Since the effect is small, due to the emission falling rapidly for  $\nu > \nu_L$ , we do not include this trend in our parameterisation. While all the fitted parameters vary on a shower-to-shower basis, variations tended to be small, so that approximating  $k_E \approx \bar{k}_E$ ,  $\beta \approx \bar{\beta}$ , etc. for individual showers is appropriate. The exception is  $k_L$ , where we find (not unexpectedly [29,31,32]) that variations from the mean fitted values  $\bar{k}_L$  are large, particularly at high energies. These fluctuations will dominate the radiation pattern in the regime where longitudinal decoherence dominates, which at the highest energies is everywhere except within a small fraction of a degree from  $\theta_C$ . We assume that at a given energy  $k_L$  is log-normally distributed about the mean  $\bar{k}_L$  as given by Eq. (11), with an energy-dependent variance in log-space of  $\sigma_{k_L}^2$ :

$$\log_{10}(k_L) \sim N(\log_{10}(\bar{k}_L), \sigma_{k_L}^2). \quad (11)$$

Fitting for  $\sigma_{k_L}$  in each medium, we find that above a characteristic energy  $E_\sigma$ , the variation in shower length increases rapidly, while below  $E_\sigma$  the variation is approximately constant and very low. This leads us to use a parameterisation for  $\sigma_{k_L}$  — Eq. (12) — similar to Eq. (10) for  $k_L$  itself:

$$\sigma_{k_L} = \begin{cases} \sigma_0 + \delta_0 \log_{10}(E/E_\sigma) & E < E_\sigma \\ \sigma_0 + \delta_1 \log_{10}(E/E_\sigma) & E > E_\sigma \end{cases} \quad (12)$$

with parameters  $\sigma_0$ ,  $E_\sigma$ ,  $\delta_0$ , and  $\delta_1$  again fitted separately to each medium, with results given in Table 6. These parameters complete the parameter set with which we characterise electromagnetic showers.

Medium	$\bar{k}_E$	$\bar{k}_R$	$\bar{\alpha}$	$\bar{\beta}$
Ice	$4.65 \cdot 10^{-16}$	1.54	1.37	2.74
Salt	$3.12 \cdot 10^{-16}$	1.39	1.32	2.70
Regolith	$3.37 \cdot 10^{-16}$	1.50	1.32	2.79
Megaregolith	$3.46 \cdot 10^{-16}$	1.47	1.32	2.68

Table 4

Fitted shower parameters, as defined by Eqs. (7)-(9). Units for  $\bar{k}_E$  are V/cm/MHz<sup>2</sup>.  $\bar{k}_L$  (not shown in this table) was fitted to Eq. (10) with parameters given in Table 5.

Medium	$\log_{10} k_0$	$\log_{10} (E_{\text{LPM}}^*/\text{eV})$	$\gamma_0$	$\gamma_1$
Ice	1.52	16.61	$5.59 \cdot 10^{-2}$	0.39
Salt	1.71	16.44	$8.21 \cdot 10^{-2}$	0.44
Regolith	1.58	16.40	$6.71 \cdot 10^{-2}$	0.43
Megaregolith	1.57	16.38	$6.39 \cdot 10^{-2}$	0.46

Table 5

Parameters of the fit for  $\bar{k}_L$ , as defined by Eq. (10).

Medium	$\sigma_0$	$\log_{10} (E_\sigma/\text{eV})$	$\delta_0$	$\delta_1$
Ice	$3.39 \cdot 10^{-2}$	14.99	$\sim 0$	$2.25 \cdot 10^{-2}$
Salt	$4.98 \cdot 10^{-2}$	14.99	$\sim 0$	$2.40 \cdot 10^{-2}$
Regolith	$5.04 \cdot 10^{-2}$	14.98	$\sim 0$	$2.44 \cdot 10^{-2}$
Megaregolith	$5.19 \cdot 10^{-2}$	14.99	$\sim 0$	$2.50 \cdot 10^{-2}$

Table 6

Parameters relating to  $\sigma_{k_L}$  (the variation of  $\log_{10}(k_L)$  about  $\log_{10}(\bar{k}_L)$ ) as defined by Eq. (11) and Eq. (12).

#### 4.2 Comparison with other calculations and Discussion

Comparisons of our parameter estimates with those from previous simulations are only possible for ice over the entire energy-range, and for salt and the regolith for  $E_0 < 100$  TeV. The parameter estimates obtained by Alvarez-Muñiz et al. [16] for ice and the regolith at low energies agree with our results to within  $\sim 3\%$  for  $\bar{k}_E$ , and within 10% for  $\bar{k}_R$  and  $\bar{\alpha}$  in all media. The larger differences in the shape parameters are not unexpected, since these vary more on a shower-to-shower basis, and the fitted values are partially subject to the fitting procedure.

Comparisons of  $\bar{k}_L$  and  $\bar{\beta}$  with the estimates in Ref. [16] must be viewed with caution. Here these parameters have a slightly different meaning to those obtained in [16], since we retain the transverse decoherence term  $d_R$  from Eq. (5) at all angles. A better comparison is to the one-dimensional results of Alvarez-Muñiz et al. [29], who found a parameter set approximately corresponding to  $\{\log_{10}(E_{LPM}^*), \gamma_1, \gamma_2\} = \{16.15, 0.03, 0.3\}$ , whereas here we find (for our full 3-D simulation) the set  $\{16.69, 0.04, 0.45\}$ . The most important update to this parameterisation is the steeper increase in shower length with energy, and hence narrower emission at the highest energies.

In Fig. 7, we plot the radiated emission at various angles from a 100 EeV shower in ice (Fig. 7(a)) and a 100 EeV shower in the megaregolith (Fig. 7 (b)), which is the least “ice-like” medium. For each shower, we show (i): the spectra from a particular simulated shower as calculated by ZHS-thinned, obtained using three simultaneous calculations with  $(E_{\min}, f_L) = (100 \text{ MeV}, 10^7)$  – we also plot (ii): the fitted spectrum for that particular shower using the functional forms and fitting procedure described in this paper, (iii): the parameterisations presented here, using three values of  $k_L$  ( $k_L - \sigma_{k_L}$ ,  $\bar{k}_L$ , and  $\bar{k}_L + \sigma_{k_L}$ ), and (iv): the parameterisation of Alvarez-Muñiz et al. in Ref. [19] for ice and extrapolated from its known range of validity (100 TeV - 1 PeV at most), used as published in ice in the top panel, and scaled as per James et al. [25] for the megaregolith. Also shown (v) are the spectra calculated by Fourier-transforming the distribution of excess tracklength from each of the three simulated showers [19], normalising by our fitted constants  $\bar{k}_E$ , and multiplying by the lateral decoherence factor  $d_R$ .

The broad range of expected spectra given by the variation in  $k_L$  is immediately apparent: whereas we have chosen a typical shower in the megaregolith, the shower in ice is significantly shorter than average – more than  $1 \sigma$  – as evinced by the high turn-over frequencies. It is also clear that previous parameterisations which were not valid away from the Cherenkov angle for energies above  $E_{LPM}$  overestimate the width of the Cherenkov cone at the highest energies. This emphasises the need for direct simulations such as those presented in this work. The overestimation is also greater in the megaregolith than in ice. The effect on the sensitivity of neutrino-hunting experiments is not likely to be large however, since the shorter hadronic (and subsequent electromagnetic) cascades expected from neutral-current  $\nu$ -interactions are more readily detectable.

The similarity of our parameter estimates for the regolith and megaregolith (identical chemical composition, different densities and refractive indices) reflects the suitability of the scaling inherent in the box-model of shower development. The largest relative parameter difference between these media was 7%, and in particular, the estimated values for  $k_E$  (which have shown the greatest variation [16]) were within 3%. This compares to differences between

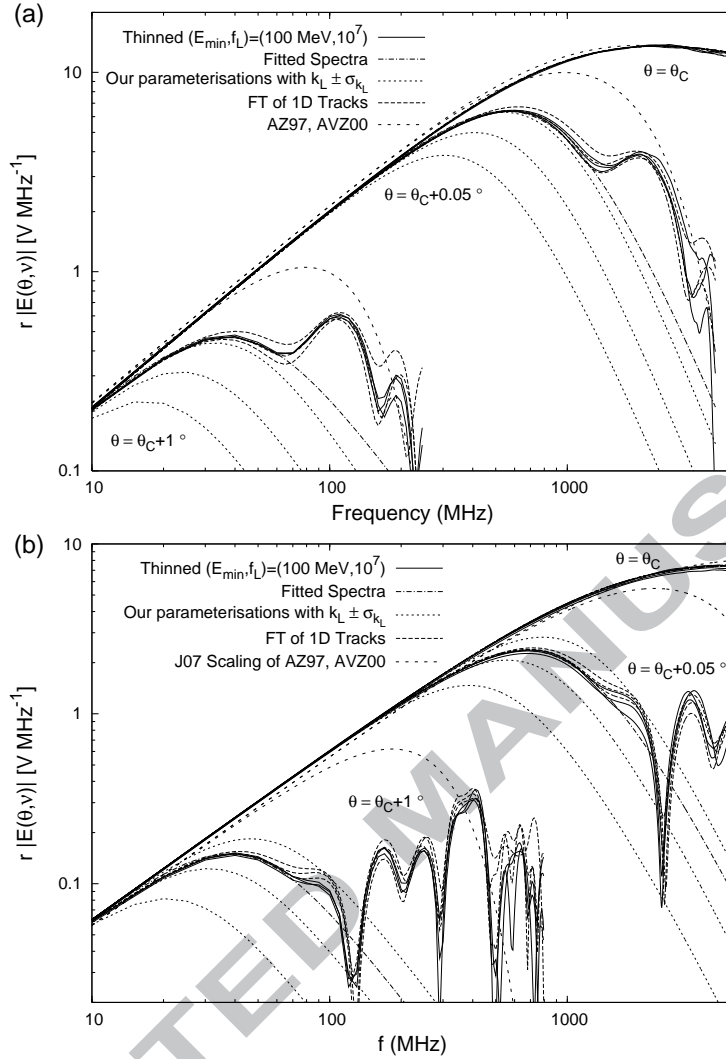


Fig. 7. 100 EeV electron showers in ice (top panel), and the lunar megaregolith (bottom). Shown are both direct calculations of the spectra and parameterisations (see text for details).

salt-regolith parameter estimates (20%) and ice-anything ( $> 30\%$ ), indicating that the variation due to subtle compositional effects, rather than easily-characterisable bulk properties. We therefore expect that the box-model can be used with confidence to scale results for standard ice to variants thereon found deeper in the Antarctic ice sheet, or equally from regolith/megaregolith to intermediate/transitional layers.

## 5 Coherent Cherenkov Radiation from Hadronic Showers

The thinned-ZHS code developed in this work is currently unable to produce simulations of hadronic showers. These are of utmost importance for neutrino

detection since they are induced by all neutrino flavors in neutral current (NC) interactions, as well as in the hadronic vertex of charged current (CC) interactions of muon and tau neutrinos. Although on average only  $\sim 20\%$  of the neutrino energy is carried by the hadronic shower at ultra-high energy, hadronic showers are known to be less affected by the LPM effect [34] and their Cherenkov emission does not suffer from the shrinking of the Cherenkov cone which would otherwise reduce the solid angle for observation. On the other hand mixed showers induced in CC electron neutrino interactions are composed of a purely electromagnetic shower – produced by an energetic electron carrying on average  $\sim 80\%$  of the energy of the neutrino – and a hadronic shower initiated by the debris of the interacting nucleon. The advantage for neutrino detection of these types of interactions is that all the neutrino energy is channeled into the resulting shower, however the observation of the electromagnetic shower is expected to be very difficult because the LPM effect shrinks the angular distribution of the electric field reducing dramatically the available solid angle for detection. For these reasons experiments aiming at detecting neutrinos using the radio technique gain most of their acceptance from neutrino-induced hadronic showers [7,5,37].

As stated above, hadronic showers are less affected by the LPM effect, and their efficiency of emission of coherent Cherenkov radiation at high energy has been shown to be similar to that of electromagnetic showers [36]. Besides, at high energy, a very large fraction of the energy of the hadronic showers goes into its electromagnetic component [34]. For these reasons and although our parameterizations are only strictly valid for purely electromagnetic showers, those at energies below  $E_{\text{LPM}}$  can also serve to model hadronic showers in an approximate manner, after properly scaling the normalization of the electric field in the fully coherent region with the energy of the induced shower. Despite this fact, clearly accurate simulations of mixed and hadronic showers with energies above  $E_{\text{LPM}}$  in different dense media are needed. We are extending our efforts to neutrino-induced showers and we are currently implementing the algorithms for radio emission used in the ZHS code in external codes that are able to simulate with great detail neutrino-induced showers in dense media [38]. Results of this ongoing work will be presented elsewhere [39]. We note however that a significant part of a 'hadronic' shower is actually the electromagnetic component which in a dense medium develops at high energies (mostly) from the decay of neutral pions. Therefore the thinning of electromagnetic showers is a significant first step towards the calculation of the emission from UHE hadronic showers.

## 6 Conclusions

We have used thinning techniques to develop a robust version of the ZHS code able to calculate the frequency spectrum of coherent Cherenkov radiation from ultra-high energy (UHE) electromagnetic showers in an arbitrary dense medium. Using this code, we have identified a range of thinning parameters able to produce accurate results with a large reduction in computing time, and extended the energy range at which full calculations of the radiated spectrum are possible from 100 TeV to 100 EeV. This has enabled us to analyse the structure of highly-elongated LPM-affected showers in unprecedented detail, and the parameterisations we have developed should prove a useful and accurate tool in simulations of UHE neutrino detection using the radio technique.

In particular, we have shown that the spectral fall-off due to longitudinal decoherence occurs at a lower frequency than scaling of results from lower energies would imply, and for the first time give a method of including LPM-induced fluctuations into the parameterisation by varying the length parameter  $k_L$ .

## 7 Acknowledgments

J.A-M and E.Z thank Xunta de Galicia (PGIDIT 06 PXIB 206184 PR) and Consellería de Educación (Grupos de Referencia Competitivos – Consolider Xunta de Galicia 2006/51); Ministerio de Ciencia e Innovación (FPA 2007-65114 and Consolider CPAN) and Feder Funds, Spain. J.A-M acknowledges the hospitality of the Univ. of Adelaide (Australia) and of ATCA (Australian Telescope Compact Array) where part of this work was done. We thank CESGA (Centro de SuperComputación de Galicia) for computing resources. C.W.J and R.J.P would like to thank the Univ. Santiago de Compostela for their hospitality, and acknowledge the support of the Australian Research Council’s Discovery Project funding scheme (projects number DP0559991 and DP0881006). We thank R.A. Vázquez for helpful discussions.

## References

- [1] T.K. Gaisser, F. Halzen, T. Stanev, Phys. Rep. **258**, 173 (1995); Phys. Rep. **271**, 355 (1995) (erratum).
- [2] J.G. Learned, K. Mannheim, Ann. Rev. Nucl. Sci. **50**, 679-749 (2000).
- [3] F. Halzen, D. Hooper, Rep. Prog. Phys. **65**, 1025 (2002).

- [4] G.A. Askar'yan, Soviet Physics JETP **14**, **2**, 441 (1962); Soviet Physics JETP **48**, 988 (1965).
- [5] I. Kravchenko *et al.* Phys. Rev. D **73**, 082002 (2006); Astropart. Phys. **19**, 15 (2003).
- [6] T. Hankins *et al.* Mon. Not. Royal Astron. Soc. **283**, 1027 (1996); C.W. James *et al.* Mon. Not. Royal Astron. Soc. **379**, 1037 (2007).
- [7] S. Barwick *et al.* Phys. Rev. Lett. **96**, 171101 (2006).
- [8] P.W. Gorham *et al.* Phys. Rev. Lett. **93**, 041101 (2004).
- [9] O. Scholten *et al.* Astropart. Phys. **26**, 219 (2006).
- [10] C.W. James *et al.*, Proc. 30<sup>th</sup> International Cosmic Ray Conference, Merida, Mexico (2007).
- [11] P.W. Gorham *et al.* Phys. Rev. E **62**, 6, 8590 (2000).
- [12] D. Saltzberg *et al.*, Phys. Rev. Lett. **86**, 2802 (2001).
- [13] P. Miocinovic *et al.* Phys. Rev. D **74**, 043002 (2006).
- [14] P.W. Gorham *et al.* Phys. Rev. D **72**, 023002 (2005).
- [15] P.W. Gorham *et al.* Phys. Rev. Lett. **99**, 171101 (2007).
- [16] J. Alvarez-Muñiz, E. Marqués, R.A. Vázquez, E. Zas, Phys. Rev. D **74**, 023007 (2006).
- [17] E. Zas, F. Halzen, T. Stanev, Phys. Rev. D **45**, 362 (1992).
- [18] J. Alvarez-Muñiz, R.A. Vázquez, E. Zas, Phys. Rev. D **61**, 023001 (1999).
- [19] J. Alvarez-Muñiz, R.A. Vázquez, E. Zas, Phys. Rev. D **62**, 063001 (2000).
- [20] R.V. Buniy, J.P. Ralston, Phys. Rev. D **65**, 016003 (2002).
- [21] A.M. Hillas, Nucl. Phys. B (Proc. Suppl.) **52B**, 29 (1997).
- [22] M. Kobal, Astropart. Phys. **15**, 259 (2001).
- [23] J. Alvarez-Muñiz, E. Marqués, R.A. Vázquez, E. Zas, Phys. Rev. D **67**, 101303 (2003).
- [24] L. Landau, I. Pomeranchuk, *Dokl. Akad. Nauk SSSR* **92**, 535 (1953); **92**, 735 (1935); A.B. Migdal, Phys. Rev. **103**, 1811 (1956); Zh. Eksp. Teor. Fiz. **32**, 633 (1957) [Sov. Phys. JETP **5**, 527 (1957)].
- [25] C.W. James, R.J. Protheroe, Astropart. Phys. **30**, 318 (2009).
- [26] D.S. Gorbunov, G.I. Rubstov, S.V. Troitsky, Phys. Rev. D **76**, 043004 (2007).
- [27] T. Stanev *et al.*, Phys. Rev. D **25**, 1291 (1982).

- [28] K. Greisen, in: Prog. of Cosmic Ray Phys., ed. J.G. Wilson, Vol. III, (North Holland Publ. Co., Amsterdam, 1956) p.1., K. Kamata, J. Nishimura, Prog. Theor. Phys. (Kyoto) Suppl. **6**, 93 (1958).
- [29] J. Alvarez-Muñiz, E. Zas, Phys. Lett. B **411**, 218 (1997).
- [30] S. Razzaque *et al.* Phys. Rev. D **65**, 103002 (2002); S. Razzaque *et al.* Phys. Rev. D **69**, 047101 (2004).
- [31] J.P. Ralston, D.W. McKay, Proc. of High Energy Gamma-Ray Astronomy Conference (Ann Arbor, Mi 1990), ed. James Matthews (AIP Conf. Proc. 220) p.295.
- [32] E. Konishi, A. Adachi, N. Takahashi, A. Misaki, J. Phys. G: Nucl. Part. **17** 719 (1991).
- [33] S.R. Klein, 44<sup>th</sup> Workshop on QCD at Cosmic Energies: The Highest Energy Cosmic Rays and QCD, Erice, Italy, 2004. arXiv:astro-ph/0412546
- [34] J. Alvarez-Muñiz, E. Zas, Phys. Lett. B **434**, 396 (1998)
- [35] R. Protheroe and R.P. Johnson, Astropart. Phys. **4** (1996) 253; R. Engel, D. Seckel and T. Stanev, Phys. Rev. D **64** (2001) 093010; D. Allard *et al.* JCAP **9** (2005) 5.
- [36] S. Hussain and D.W. McKay, Phys. Rev. D **70**, 103003 (2004).
- [37] J. Alvarez-Muñiz, C.W. James, R. Protheroe and E. Zas, to appear in Procs. of the 31<sup>st</sup> International Cosmic Ray Conference, Lodz, Poland, 2009.
- [38] M. Tueros *et al.*, see talk given at Rencontres de Moriond 2009, available at <http://moriond.in2p3.fr/J09/schedule2.html>
- [39] J. Alvarez-Muñiz *et al.* in preparation.